Development, Analysis and Experimental Realization of a Direct-Drive Helical Motor

Issam A. Smadi, *Member, IEEE*, Hiroko Omori, and Yasutaka Fujimoto, *Member, IEEE*

***Abstract*—Safety issue is great concern for rehabilitation robots that are expected to contribute to future aging society. Appropriate compliance is required for their joints. However, combination of servomotors and high-ratio gears, such as harmonic gears makes the joint of robots nonbackdrivable. The nonbackdrivability causes lack of adaptability and safety. On the other hand, Conventional direct-drive systems, including linear motors, are relatively big for such application. This paper presents development and analysis of compact high backdrivable direct-drive linear actuator. The motor consists of a helical structure stator and mover. The mover does not contact the stator and moves helically in the stator under a proper magnetic levitation control. Thus, the motor realizes direct drive motion without mechanical gears. Decoupling control is proposed and integrated with disturbance observer to achieve robustness against model uncertainties and input disturbance. The main contribution of this paper is to experimentally realize the direct-drive feature of the helical motor.**

***Index Terms*— Magnetic levitation, motion control, electric machines, AC motors, permanent magnet machines, motor drives, robust control, position control, current control, linear feedback control systems.**

NOMENCLATURE

$c(\theta)$ Spatial distribution for magnetomotive force of permanent magnet.
d_x, d_θ Thrust-force and torque disturbances including modeling error.
D, D_τ friction coefficient for linear/rotational motion.
f Thrust force of mover generated by magnetic circuit part (A) in Fig. 6.
f_{all} Thrust force of mover.
Φ_i Interlinkage flux for current I_i, $i \in \{u, v, w, m\}$.
I_i i-phase current, $i \in \{u, v, w\}$.
I_m Equivalent magnetization current of permanent magnet.
I_d, I_q d-axis, q-axis current.
J Moment of inertia of mover.
k Fundamental Fourier component of $c(\theta)$.
K_f Thrust-force constant.
K_τ Torque constant.
K_g Equivalent axial stiffness due to permanent magnet.
L Inductance matrix.
L_d, L_q d-axis, q-axis inductance.
l_g Nominal length of air gap.
l_m Width of magnet.
l_p Lead length of screw.
μ_0 Permeability in vacuum.
μ_m Permeability of permanent magnet.
M Mass of mover.
n Ampere-turn.
ν_x Virtual acceleration input of linear position controller.
ν_{xg} Virtual acceleration input of gap regulator.
ν_θ Virtual acceleration input of rotation controller.
p Number of pole pairs per 360° mechanical angular displacement.
P_d, P_q d-axis, q-axis permeance.
θ Mechanical rotation angle of mover.
R_g Reluctance of forward side air gap for an area of a phase winding.
R_g' Reluctance of backward side air gap for an area of a phase winding.
R_m Reluctance of permanent magnet for an area of a phase winding.
R_s Resistance of windings.
S Gap area per 360° mechanical angular displacement.
τ Torque of mover generated by magnetic circuit part (A) in Fig. 6.
τ_{all} Torque of mover.
u_x Virtual force input for linear motion.
u_θ Virtual torque input for rotational motion.
V_i voltage at i-phase windings, $i \in \{u, v, w\}$.
x Linear position of mover.
x_g Displacement of air gap.
Ψ_m Field flux by the permanent magnet.

Manuscript received February 1, 2011; revised April 8; accepted April 20, 2011. This work was supported by KAKENHI under Grant 1967003.

I. A. Smadi was with the Department of Electrical and Computer Engineering, Yokohama National University, Yokohama 240-8501, Japan. He is now with the Fuji Electric Systems Co., Ltd., Tokyo 191-0852, Japan (e-mail: smadi@fujilab.dnj.ynu.ac.jp)

H. Omori was with the Department of Electrical and Computer Engineering, Yokohama National University, Yokohama 240-8501, Japan. She is now with the Toyo Electric Mfg. Co., Ltd., Yokohama 236-0004, Japan (e-mail: omori@fujilab.dnj.ynu.ac.jp)

Y. Fujimoto is with the Department of Electrical and Computer Engineering, Yokohama National University, Yokohama 240-8501, Japan (phone: +81-45-339-4175; fax: +81-45-338-1157; e-mail: fujimoto@ynu.ac.jp)

I. Introduction

Direct-drive system is, almost, free from backlash and friction and easy to realize for precise, high-speed, and safe motion. Therefore, from the viewpoint of controllability, the direct-drive systems are suitable for robotics applications. On the other hand, safety issue is great concern for rehabilitation robots that are expected to contribute to future aging society [1]-[3]. Appropriate compliance is required for their joints. However, in robotics application a combination of servomotors and high ratio gears, such as harmonic gears, is widely used in practice. During transmission by the high ratio gear loss of torque and power occurs and the joint of robots becomes nonbackdrivable which causes lack of adaptability and safety.

To recover the backdrivability, several joint mechanisms and controls were proposed [4]-[12]. The direct-drive system for robotic application, firstly reported in [4], avoids friction loss and realizes good controllability. Less-friction direct-drive system enables sensorless force control based on disturbance observer [5]. However, the mass and volume of the robot becomes too big and not suitable for practical applications. Another sensorless force control for a robot manipulator with geared actuators was reported in [6]. The bandwidth of the controlled system was limited due to friction of gears. In order to improve the performance of force control system, several solutions were proposed. One is disturbance observer combined with an accelerometer proposed in [7], which enhances the sensing bandwidth. Another solution is a twin-drive system reported in [8], which cancels the static friction of two geared motors each other by using a differential gear system. The static friction does not appear in the total output of the joint system. Some actuators put elastic mechanism between the output and gears [9]-[12]. The elasticity improves stability and safety but decreases controllability in high frequency domain. A two-stage actuator system [10] overcomes this drawback but the system becomes complicated.

Conventional linear motors provide direct-drive motion and eliminate mechanical transmission devices. Recently, many works on permanent magnet (PM) linear synchronous motors have been reported [13]-[28]. Due to low thrust per unit volume characteristic, the size of the system becomes relatively big for high-thrust application. A high thrust density linear motor (HDL) has been proposed in [13][14]. From the viewpoint of a thrust per air gap area HDL can generate a thrust force two times higher than conventional PM synchronous motor and six times than linear induction motors [13]. PM tubular linear (PM-TL) motor is another example of high thrust-force linear motor [15]-[23]. The design optimization and magnet arrangement of the PM-TL motor was discussed in [15], and the quasi-Halbach magnetized magnet type was developed in [16]-[18]. Short-stroke single-phase PM-TL motor was developed in [19] to drive a reciprocating vapor compressor. Comparisons among different PM-TL motor configurations were reported in [20]. The finite-element analysis of the coupled magnetothermal behavior of PM-TL motor was presented in [21] revealing valuable information for the design optimization process. Sensorless control for PM-TL motor based on pulsating voltage injection was presented in [23]. Controls of PM linear motors were reported in [23]-[28]. Another linear actuators such as a PM linear oscillatory machine [29], linear switched reluctance motors [30][31], a dual solenoid actuator [32], a hybrid magnetic suspension actuator [33], a linear piezoelectric ceramic motor [34], and shape memory alloy actuators [35][36] were investigated.

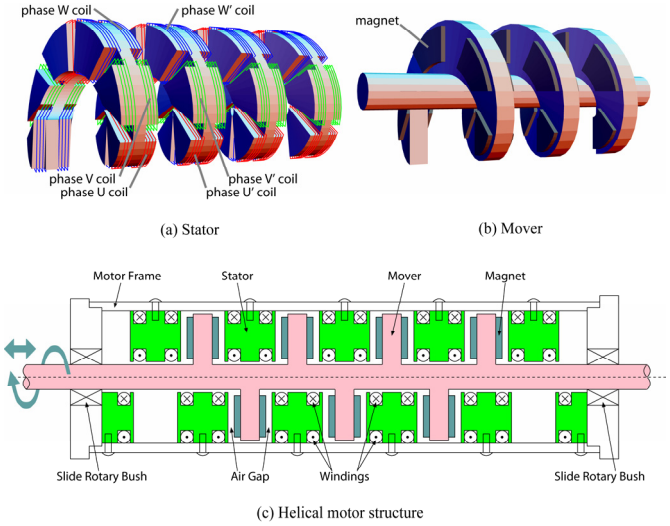

Fig. 1. Preliminary structure of a helical motor. (a) Stator with three-phase windings. (b) Mover with permanent magnets. (c) Cross section view.

There are several approaches to improve thrust-force of linear motors. Roughly speaking, thrust-force is directly proportional to gap area and inversely proportional to gap length. A method to expand gap area without increasing volume is to design a motor of a special three-dimensional structure.

Recently, a novel high-thrust quasi-direct-drive linear actuator with helical (spiral) structure has been developed [37]. This motor is an axial-gap helical motion permanent magnet (PM) motor. The motor has relatively high thrust-force characteristics thanks to the wide gap area on the helical 3-D structure. For feasibility study open loop (synchronous drive) control was carried out and it has been confirmed in [37] that helical motor is almost close to the latest state of the art in linear motor technology. By introducing a ball-screw at the axis of the mover, the magnetic levitation control was not necessary for the first prototype reported in [37]. As a result, the system only has a quasi-direct-drive feature.

The motor developed in this paper does not utilize a ball-screw mechanism. Therefore, a proper magnetic levitation control (gap control) is needed to achieve full direct-drive feature of the motor. Moreover, the helical structures of the first prototype were approximately realized by combining almost flat units. However, the helical structures of the proposed motor are fully helical shape. Helical motor consists of a helical stator and a helical mover with PM. The mover does not contact the stator and moves helically in the stator under a proper magnetic

levitation control. Thus, the motor realizes direct-drive motion without mechanical gears. Fig. 1 depicts helical motor's basic structure. Slots are provided for winding on the surface of the stator. PMs are attached on the surface of the mover. The flux in the axial direction is generated by the three phases winding in the stator slots. Thrust load of the mover is controlled directly by the electromagnetic force while two slide-rotary bushes support the radial load.

Simulation results of direct-drive system have been presented in [38]-[41]. Initial, basic, experimental result of magnetic levitation control has been done in [42] neglecting the linear position dynamic. Realization of direct-drive motion of helical motor did not achieve in [42]. In this paper, decoupling control is proposed, to decuple the gap dynamic from the linear position dynamic, and integrated with disturbance observer to achieve robustness against model uncertainties and input disturbance. The main contribution of this paper is to experimentally realize the direct-drive feature of the proposed motor.

The concept of the helical motor under the levitation control proposed in this paper is similar to existing levitation motors [43]-[49]. There are axial-gap type [43], radial-gap type [44]-[46], and linear levitation [47] motors. An application to blood pump is reported in [48][49]. However, structure of the proposed motor is completely different from existing levitation motors.

On the other hand, various types of a helical-motion motor capable of producing rotary, linear, or helical motion have been proposed in [50]-[56]. There are induction-type [50]-[53], reluctance-type [54], and permanent-magnet-type [55]-[56] motors. Another variation is a 1-DOF actuator with rotary type stepping motor drive system applied to a mover with double-helical PM [57]. All of the aforementioned helical motors are radial-gap motors. Therefore the gap area of these motors are basically same as tubular linear motors and there is no gain of thrust-force per unit volume.

This paper is organized as follows. In Section II, the structure and modeling of helical motor is presented. The proposed direct-drive control that decouples the gap dynamic from the linear position dynamic is given in Section III. Experimental results are given in Section IV. Finally, conclusions are given in Section V.

II. Modeling of Helical Motor

A. Prototype

The helical-shape stator yoke shown in Fig.2(a) is made of soft magnetic composite. A helical-shape Nd-Fe-B magnet is shown in Fig. 2(b). Internal structure of the stator is shown in Fig. 3(a). The Nd-Fe-B magnets are attached on the mover yoke which is made of silicon steel, as shown in Fig. 3(b). Precise helical shapes of the stator and mover enable uniform short length of air-gap and avoid concentration of stress when the mover touches down to the stator. Moreover, Teflon sheets have been installed on the surface of the magnet to avoid direct iron-to-iron contact of the stator and mover if the axial control is lost.

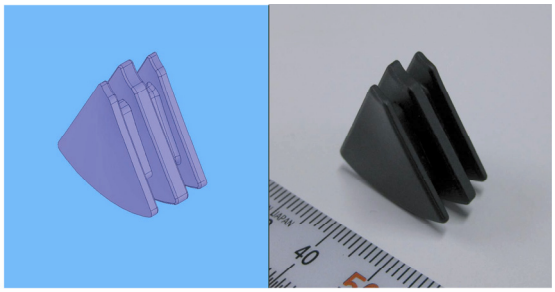

(a)

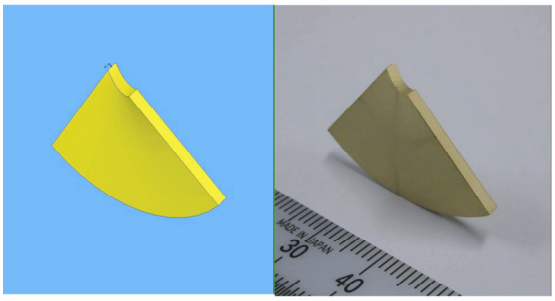

(b)

Fig. 2. Stator yoke and magnet of the motor. (a) A helical shape stator yoke. (b) A helical shape Nd-Fe-B magnet

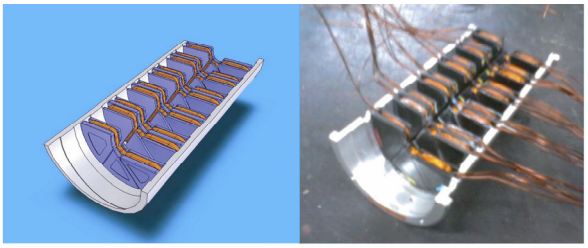

(a)

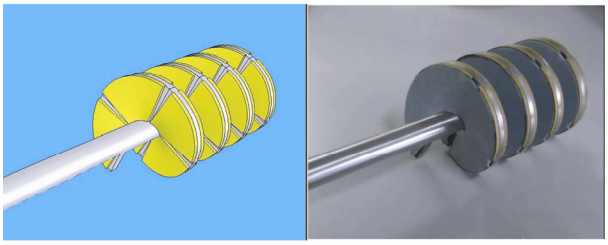

(b)

Fig. 3. Stator and the mover of the motor. (a) Internal structure of the stator. (b) Helical shape mover.

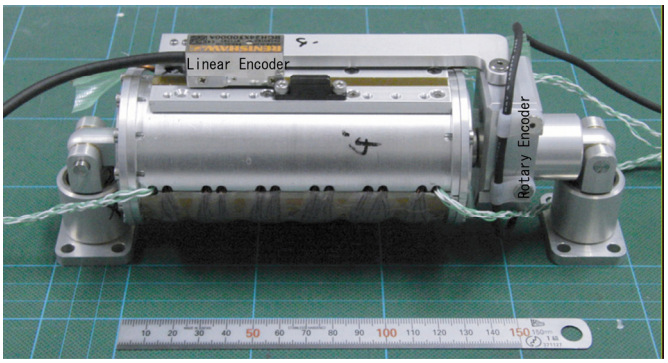

Fig. 4. Exterior of a helical motor.

Exterior of the helical motor is shown in Fig. 4. A rotary

encoder and linear encoder attached to the motor measure the linear position x and rotation angle θ for control. Displacement of the air gap x_g is computed by using these measurements as follows.

$$x_g = x - \frac{l_p}{2\pi}\theta \tag{1}$$

where, l_p is lead length of screw.

B. Permeance model

Throughout this paper, the edge effect is ignored and it is assumed that the permeability of the permanent magnet μ_m is equivalent to the permeability in vacuum μ_0. Using permeance model of the helical motor for 360° electrical angular displacement in polar coordinates, voltage equation, thrust-force and torque equations are analytically driven in this section. Fig.5 shows polar coordinates expression of the motor. From this model, a simple magnetic circuit is obtained as shown in Fig. 6. $R_g = 3p(l_g - x_g)/S\mu_0$ is reluctance of forward side air gap for an area of each phase windings, where S is the gap area of cross section of the cylinder, l_g is nominal length of the air gap. $R'_g = 3p(l_g + x_g)/S\mu_0$ is reluctance of backward side air gap. $R_m = 3pl_m/S\mu_m$ is reluctance of a PM, where l_m is magnet width and p stands for number of pole pairs per 360° mechanical angular displacement. $c(\theta) = k\cos(\theta)$ is a spatial function of magnetomotive force of the PM , where k is the fundamental component.

Two independent three-phase inverters are required for driving the helical motor. One inverter controls part (A) circuit and the other controls part (B) circuit. Assume that equivalent field magnet windings is located instead of the permanent magnet. In part (A) of the magnetic circuit, the interlinkage flux $\Phi = [\Phi_u, \Phi_v, \Phi_w, \Phi_m]^T$ for each current is obtained as $\Phi = LI$ where $I = [I_u, I_v, I_w, I_m]^T$ is the current vector and L is the inductance matrix. Φ_m and I_m represent interlinkage flux and equivalent magnetization current for the field magnet windings, respectively. For salient-mover machine a mutual inductance between n_i-turns windings at position θ_i and n_j-turns windings at position θ_j is given by

$$\begin{aligned} L_{ij} = {} & P_d n_i n_j \cos(\theta_i - p\theta)\cos(\theta_j - p\theta) \\ & + P_q n_i n_j \sin(\theta_i - p\theta)\sin(\theta_j - p\theta) \end{aligned} \tag{2}$$

for $0 \le i, j \le 3$ where $n_0 = n_1 = n_2 = n$, $n_3 = n_m = 3k/2$, $\theta_0 = 0$, $\theta_1 = 2\pi/3$, $\theta_2 = 4\pi/3$, $\theta_3 = p\theta$, and $P_d \propto 1/(l - x_g)$ and $P_q \propto 1/(l - x_g)$ is the d-, q-axis permeance, respectively. $l = l_g + l_m$ is a nominal gap between the mover iron and the stator. If the machine is not salient, then the following holds, $P_d = P_q = P = 2/3(R_g + R_m)$. Using the inductance matrix, the voltage equation, thrust-force and torque equations of the helical motor can be given as follow:

$$V = RI + L\frac{dI}{dt} + \dot{\theta}\frac{\partial L}{\partial \theta}I + \dot{x}\frac{\partial L}{\partial x}I \tag{3}$$

$$f = \frac{1}{2}I^T\frac{\partial L}{\partial x}I \tag{4}$$

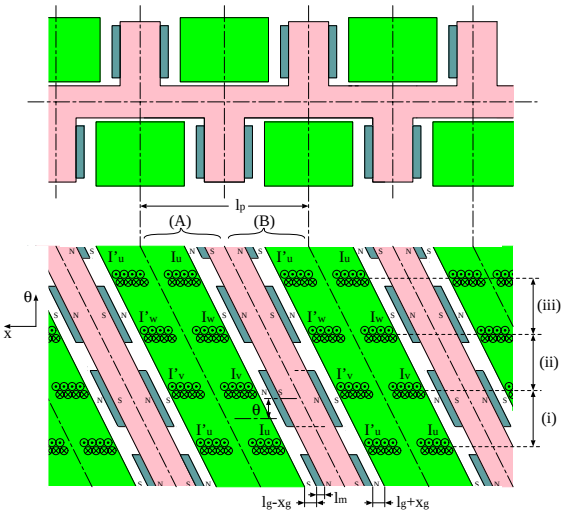

Fig. 5. A helical motor in polar coordinates.

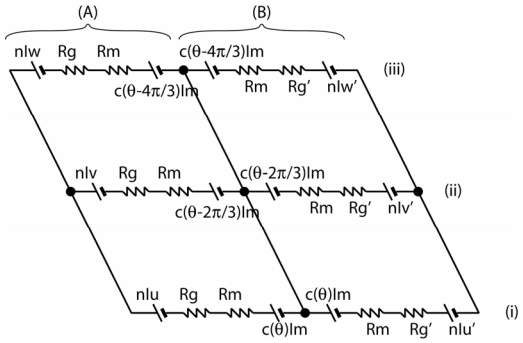

Fig. 6. Magnetic circuit.

$$\tau = \frac{1}{2}I^T\frac{\partial L}{\partial \theta}I \tag{5}$$

where $V = [V_u, V_v, V_w, V_m]^T$ is the voltage of each windings, $R = \mathrm{diag}(R_s, R_s, R_s, 0)$ is windings resistance, f and τ are thrust-force and torque of the mover, respectively.

Equations (3)-(5) are not convenient for the control design. Therefore, dq-axis model of the helical motor is derived using the following transformation matrix.

$$C = \begin{bmatrix} \sqrt{\frac{2}{3}}c_0 & \sqrt{\frac{2}{3}}c_1 & \sqrt{\frac{2}{3}}c_2 & 0 \\ -\sqrt{\frac{2}{3}}s_0 & -\sqrt{\frac{2}{3}}s_1 & -\sqrt{\frac{2}{3}}s_2 & 0 \\ \frac{1}{\sqrt{3}} & \frac{1}{\sqrt{3}} & \frac{1}{\sqrt{3}} & 0 \\ 0 & 0 & 0 & 1 \end{bmatrix} \tag{6}$$

where $c_i = \cos(p\theta - 2i\pi/3)$ and $s_i = \sin(p\theta - 2i\pi/3)$. The dq-axis current and voltage are represented by $I_{dq} = CI$ and $V_{dq} = CV$ where $I_{dq} = [I_d, I_q, I_0, I_m]^T$ and $V_{dq} = [V_d, V_q, V_0, V_m]^T$. I_d, I_q, I_0, V_d, V_q, and V_0 are d-axis,q-axis, and zero-phase current/voltage, respectively. V_m is voltage of equivalent field magnet windings of the PM, respectively. Finally, after some algebraic arrangements and observing that I_m is a constant and ignoring the zero-phase dynamic the following dq-axis voltage

equation is obtained:

$$\begin{bmatrix} V_d \\ V_q \end{bmatrix} = \begin{bmatrix} R_s & 0 \\ 0 & R_s \end{bmatrix} \begin{bmatrix} I_d \\ I_q \end{bmatrix} + \begin{bmatrix} L_d & 0 \\ 0 & L_q \end{bmatrix} \begin{bmatrix} \dot{I}_d \\ \dot{I}_q \end{bmatrix} + \Psi_m \begin{bmatrix} \dfrac{\dot{x}_g}{l - x_g} \\ p\dot{\theta} \end{bmatrix} + \left(\frac{\dot{x}_g}{l - x_g} \begin{bmatrix} L_d & 0 \\ 0 & L_q \end{bmatrix} + p\dot{\theta} \begin{bmatrix} 0 & -L_q \\ L_d & 0 \end{bmatrix} \right) \begin{bmatrix} I_d \\ I_q \end{bmatrix} \quad (7)$$

where $\Psi_m = L_{dm} I_m$ corresponds to field flux by the permanent magnet. $L_d = (3/2)n^2 P_d$ and $L_q = (3/2)n^2 P_q$ are d-axis and q-axis inductances, respectively. $L_{dm} = \sqrt{3/2}\, n n_m P_d$ is equivalent mutual inductance between d-axis stator windings and field magnet windings. Equation (7) makes use of (1) and the following relation

$$\frac{\partial L}{\partial \theta} = \left. \frac{\partial L(x_g, \theta)}{\partial \theta} \right|_{x_g = x - \frac{l_p}{2\pi}\theta} = \frac{\partial L(x_g, \theta)}{\partial \theta} - \frac{l_p}{2\pi} \frac{\partial L(x_g, \theta)}{\partial x_g} \quad (8)$$

The dq-axis voltage equation of part (B) in Fig.6 is identical to (7) taking $I_d = -I_d'$ and $I_q = I_q'$, where I_i and I_i' stand for i-axis current on forward/backward side windings, respectively, $i \in \{d,q\}$. If the above current conditions hold, i.e., $I_d = -I_d'$ and $I_q = I_q'$. Then, from (3) and (4) the total thrust-force equation and the total torque equation can be written in terms of I_{dq} current as follows:

$$f_{all} = \frac{1}{l - x_g} \left(\Psi_m I_d + \frac{L_d I_d^2 + L_q I_q^2 + L_m I_m^2}{2} \right) + \frac{1}{l + x_g} \left(\Psi_m I_d - \frac{L_d I_d^2 + L_q I_q^2 + L_m I_m^2}{2} \right) \quad (9)$$

$$\tau_{all} = 2p\left(\Psi_m I_q + (L_d - L_q) I_d I_q \right) - \frac{l_p}{2\pi} f_{all} \quad (10)$$

To this end, the equation of motion is obtained as follows:

$$M\ddot{x} = f_{all} - D\dot{x} \quad (11)$$

$$J\ddot{\theta} = \tau_{all} - D_\tau \dot{\theta} \quad (12)$$

where M is the mass of the mover, J is the inertia of the mover. D and D_τ are the friction coefficient for linear/rotational motion, respectively.

III. Direct Drive Control

For the control design, the thrust-force and torque equations are rewritten as $f_{all} = f_0 + \Delta f$ and $\tau_{all} = \tau_0 + \Delta\tau$, where

$$f_0 = K_g x_g + K_f I_d \quad (13)$$

$$\tau_0 = K_\tau I_q - \frac{l_p}{2\pi} f_0 \quad (14)$$

where $K_g = 2L_{m0} I_m^2 / l^2 > 0$ is the equivalent axial stiffness due to PM, which gives a force in favor of the displacement, i.e. destabilizing effect. $K_f = 2\Psi_{m0}/l$ is the thrust-force constant and $K_\tau = 2p\Psi_{m0}$ is the torque constant. Here, L_{m0} and Ψ_{m0} are the value of L_m and Ψ_m at $x_g = 0$, respectively.

Using (11)-(14), the helical motor model can be rewritten as

$$M_n \ddot{x} = K_{fn} I_d + K_{gn} x_g + d_x \quad (15)$$

$$J_n \ddot{\theta} = K_{\tau n} I_q - \frac{l_p}{2\pi} \left(K_{fn} I_d + K_{gn} x_g \right) + d_\theta \quad (16)$$

where subscript n denotes the nominal value. d_x and d_θ are thrust-force and torque disturbances including modeling error,

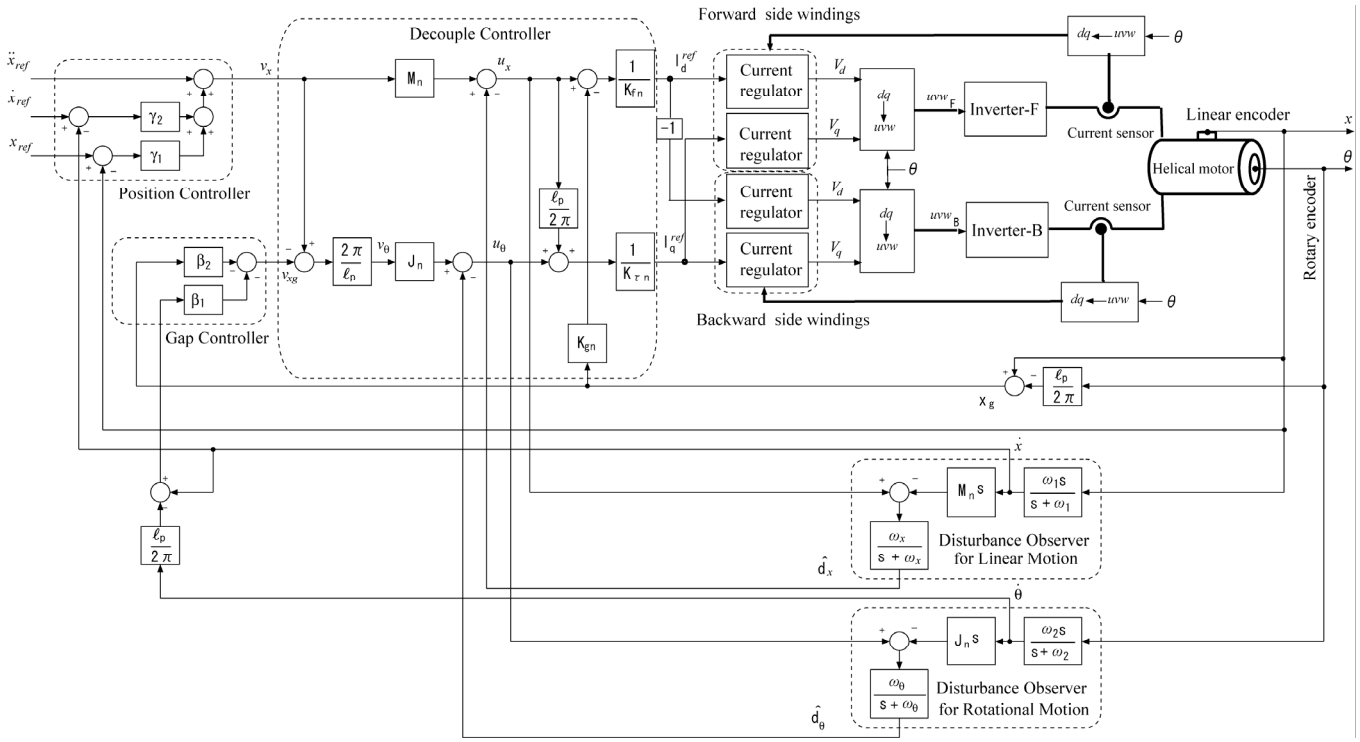

Fig. 7. Helical motor control system.

respectively.

To this end, the current in (15) and (16) can be considered as a virtual input. Therefore, the following change in the input coordinates

$$I_d^{ref} = \frac{1}{K_{fn}}\left(-K_{gn}x_g + u_x\right) \tag{17}$$

$$I_q^{ref} = \frac{1}{K_{tn}}\left(u_\theta + \frac{l_p}{2\pi}u_x\right) \tag{18}$$

transform the system into

$$M_n\ddot{x} = u_x + d_x \tag{19}$$

$$J_n\ddot{\theta} = u_\theta + d_\theta \tag{20}$$

where, u_x and u_θ are new inputs yet to be designed. The modeling error and input disturbance are compensated using disturbance observer [5]-[7] as follows

$$u_x = M_n v_x - \hat{d}_x \tag{21}$$

$$u_\theta = J_n v_\theta - \hat{d}_\theta \tag{22}$$

where,

$$v_x = \ddot{x}_{ref} + \gamma_2\left(\dot{x}_{ref} - x\right) + \gamma_1\left(x_{ref} - x\right) \tag{23}$$

$$v_{xg} = -\beta_2\dot{x}_g - \beta_1 x_g \tag{24}$$

$$v_\theta = \frac{2\pi}{l_p}\left(v_x - v_{xg}\right) \tag{25}$$

v_x is the linear position controller, v_{xg} is the gap regulator, and v_θ is the rotation controller used to decouple the linear position dynamic from the gap dynamic. The terms $\hat{d}_x$ and $\hat{d}_\theta$ are the estimated disturbances.

$$\hat{d}_x = \frac{\omega_x}{s+\omega_x}\left(u_x - M_n s\dot{x}\right) \tag{26}$$

$$\hat{d}_\theta = \frac{\omega_\theta}{s+\omega_\theta}\left(u_\theta - J_n s\dot{\theta}\right) \tag{27}$$

where s is the Laplace operator, ω_x and ω_θ are the cutoff frequencies of the disturbance observer for linear/rotation motion, respectively.

Finally, proportional-integral current regulator is used so that I_d and I_q track their reference values.

IV. Experimental Results

Extensive simulation results can be found in [38]-[41]. In this section, direct-drive feature of the helical motor is validated through experiments. Table I shows the parameters of the control system and the nominal values of the motor. Figure 4 shows the exterior of the helical motor. A rotary encoder attached to the mover shaft generates 5000 pulses per revolution. The resolution of the rotary encoder is $2\pi/20000$ using quad edge evaluation method. A linear encoder attached to the motor with resolution of 1[μm] using quad edge evaluation method. Two independent three-phase inverters, work at a 15[kHz] switching frequency, are used for driving the helical motor. One inverter (inverter-F) controls part (A) circuit and the other (inverter-B) controls part (B) circuit of Fig.6. Three-phase currents are measured using two current sensors, and captured into a DSP via A/D converter board at every sampling period of 66.7[μs]. Figure 7 depicts helical motor control system.

TABLE I
Plant and Control Parameters

p	number of pole pairs per 360° mechanical angle	2
l_p	lead length of screw	20 [mm]
K_f	thrust-force constant	6 [N/A]
K_τ	torque constant	0.25 [N.m/A]
K_g	equivalent axial stiffness	320000 [N/m]
J	moment of inertia of the mover	0.0016 [kg.m^2]
M	mass of the mover	0.5 [kg]
γ_1	proportional gain of position controller	15625
γ_2	derivative gain of position controller	250
β_1	proportional gain of gap controller	15625
β_2	derivative gain of gap controller	250
ω_x	bandwidth of disturbance observer(linear)	100 [rad/s]
ω_θ	bandwidth of disturbance observer(rotation)	100 [rad/s]
ω_1	bandwidth of linear velocity	5000 [rad/s]
ω_2	bandwidth of angular velocity	5000 [rad/s]
K_p	proportional gain of current regulator	30.303
K_i	integral gain of current regulator	30303
T_s	control sample period	66.7 [μs]
Δx	resolution of linear encoder	1 [μm]
$\Delta\theta$	resolution of rotary encoder	$2\pi/20000$ [rad]

Experiments were performed and the results are shown in Figs.8-10. Figure 8 shows the experimental results for magnetic levitation (gap) control. The mover touches down at $t < 0$[s], i.e., the gap displacement is equal to 0.35[mm]. At t=0[s], the gap control is working and the gap displacement converges to the neutral position after short transient. The d-axis current shown in Fig.8 converges to very small value as the gap displacement

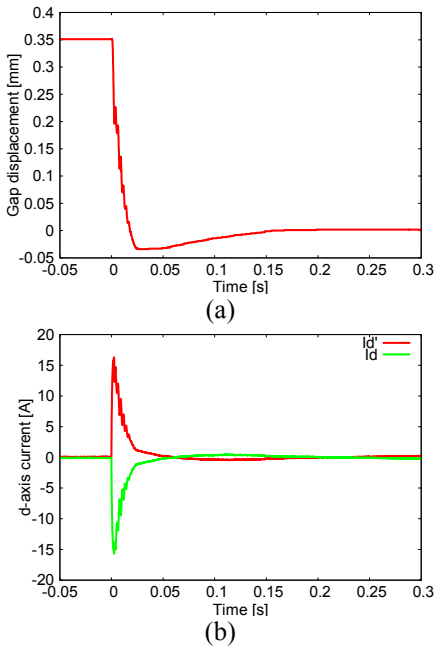

Fig. 8. Experimental results of magnetic levitation control. (a) Gap displacement, (b) d-axis current.

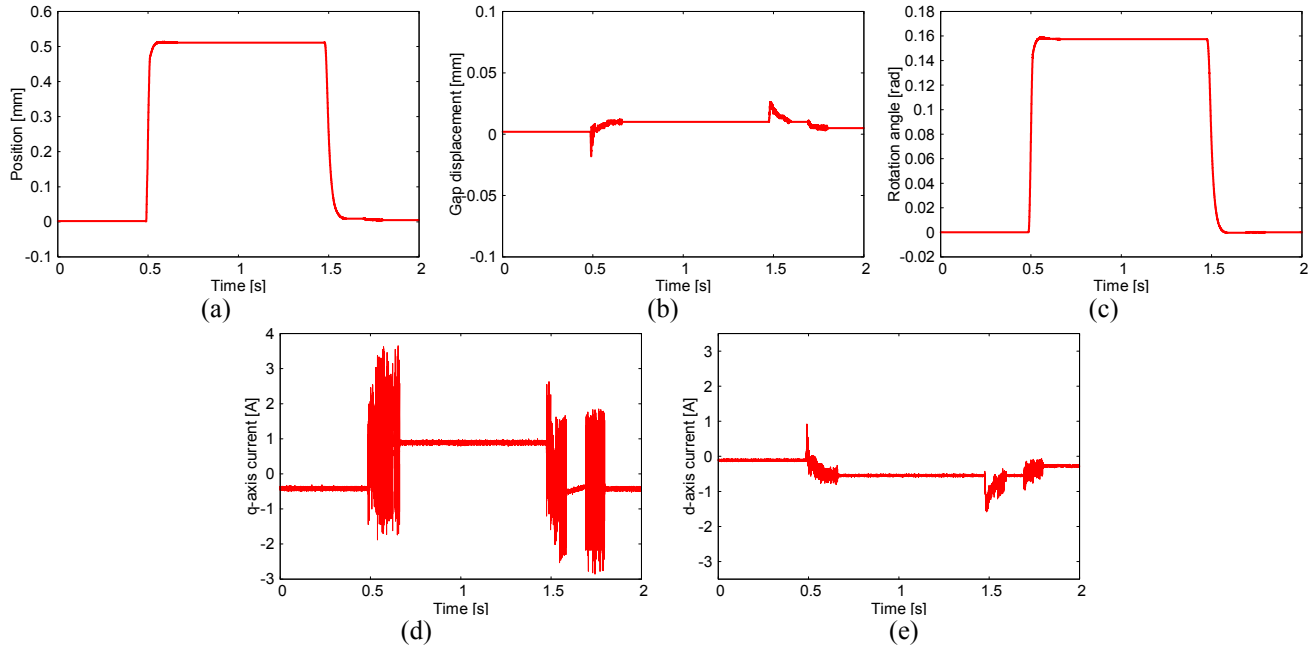

Fig. 9. Experimental results for direct-drive motion of helical motor. (a) Mover linear position. (b) Gap response. (c) Rotation angle of mover. (d) q-axis current. (e) d-axis current.

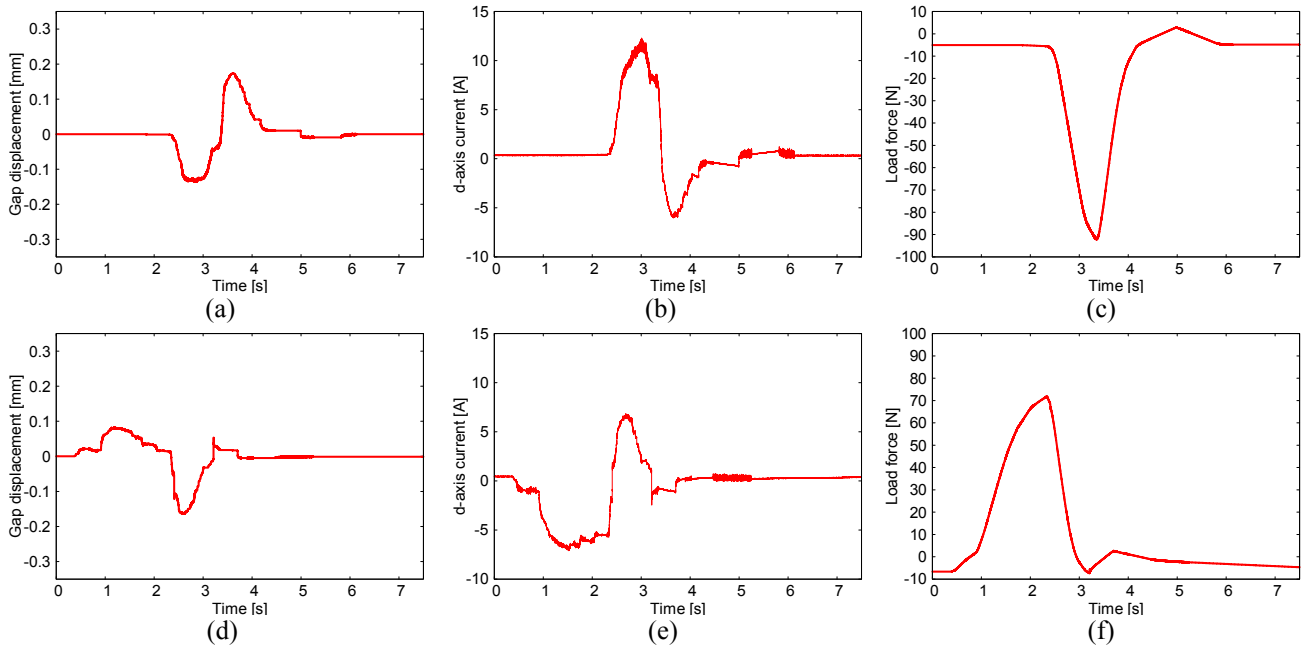

Fig. 10. Experimental results for pushing and pulling the mover. Pushing result, (a) Gap response. (b) d-axis current. (c) Load force. Pulling result, (d) Gap response. (e) d-axis current. (f) load force.

converges to the neutral position.

After the gap has been regulated, a step reference of 0.5[mm] has been given to the controller at t = 0.5[s], then at t = 1.5[s] the reference signal is changed to zero. The results are shown in Fig 9. Figure 9(a) depicts the linear position of the mover, while Fig. 9(b) and (c) shows the gap variation and the rotation angle of the mover, respectively. The d-axis current and q-axis current are shown in Fig.9 (d) and (e). From the result the linear position of the mover manage to track the reference signal by synchronously changing rotation angle while maintaining the gap displacement within a reasonable value. The axial degree of freedom follows the kinematic relation between screw pitch and angle of the mechanical screw as indicated by (1).

Figure 10 depicts the experimental results for pushing and pulling the motor mover. A force meter is used to read the actual (maximum) pushing/pulling force. For pushing case, the force meter gives 90[N] which concedes with the estimated force as shown in Fig. 10(c). The gap variation and the d-axis

current are shown in Fig.10 (a), (b), respectively. For pulling case, the force meter gives 70[N] which concedes with the estimated force as shown in Fig. 10(f). The gap variation and the d-axis current are shown in Fig.10 (d),(e), respectively.

The results from the experiments validate the motor and the proposed control

V. Conclusion

This paper presented a new type linear actuator. The motor consists of a helical structure stator and mover. The mover does not contact the stator and moves helically in the stator under a proper magnetic levitation control. Thus, the motor realizes direct drive motion without mechanical gears. Decoupling control is proposed and integrated with disturbance observer to achieve robustness against model uncertainties and input disturbance. Experimental results are given to validate the direct-drive feature of the motor.

The proposed motor is effective for driving a parallel mechanism robot and is expected to be one of the solutions for safe and high performance in robotics applications.

References

[1] G. Xu, A. Song, and H. Li, "Control system design for an upper-limb rehabilitation robot," *Advanced Robotics*, vol. 25, no.1-2, pp. 229-251, 2011.

[2] W. Yamanouchi, S. Katsura,"Variable time-space compliance control for human support," in *Proc. IEEE IECON*, pp.2093-2098, 2010.

[3] H. Vallery, J. Veneman, E. Asseldonk, R. Ekkelenkamp, M. Buss, and H. Der Kooij, "Compliant actuation of rehabilitation robots," *IEEE Robotics and Automation Magazine*, vol. 15, no. 3, pp. 60-69, 2008.

[4] H. Asada and T. Kanade, "Design of direct-drive mechanical arms," *ASME J. Vibration, Stress and Reliability in Design*, vol. 105, no.3, pp.312-316, 1983.

[5] T. Murakami, F. Yu, and K. Ohnishi, "Torque sensorless control in multidegree-of-freedom manipulator," *IEEE Trans. Ind. Electron.*, vol.40, no.2, pp.259-265, 1993.

[6] S. Katsura, Y. Matsumoto, and K. Ohnishi, "Analysis and experimental validation of force bandwidth for force control," *IEEE Trans. Ind. Electron.*, vol.53, no.3, pp.922-928, 2006.

[7] S. Katsura, K. Irie, and K. Ohnishi, "Wideband force control by position acceleration integrated disturbance observer," *IEEE Trans. Ind. Electron.*, vol.55, no.4, pp.1699-1706, 2008.

[8] C. Mitsantisuk, S. Katsura, and K. Ohishi, "Force control of human-robot interaction using twin direct-drive motor system based on model space design," *IEEE Trans. Ind. Electron*., vol. 57, no. 4, pp. 1383-1392, 2010.

[9] G. Pratt and M. Williamson, "Series elastic actuators," in *Proc. IEEE/RSJ IROS*, pp.399-406, 1995.

[10] M. Zinn, O. Khatib, B. Roth, J. K. Salisbury, "Playing it safe," *IEEE Robotics and Automation Magazine*, vol. 11, no. 2, pp. 12-21, 2004.

[11] A. Bicchi and G. Tonietti, "Fast and "soft-arm" tactics," *IEEE Robotics and Automation Magazine*, vol. 11, no. 2, pp. 22-33, 2004.

[12] A. Bicchi, M. Bavaro, G. Boccadamo, D. De Carli, R. Filippini, G. Grioli, M. Piccigallo, G. Tonietti, R. Schiavi, and S. Sen, "Physical human-robot interaction: dependability, safety, and performance," in *Proc. IEEE AMC*, pp. 9-14, 2008.

[13] Y. Muraguchi, M. Karita, H. Nakagawa, T. Shinya, and M. Maeda,"Method of measuring dynamic characteristics for linear servo motor andcomparison of their performance," in *Proc. LDIA*, pp. 204-207 , 1998.

[14] M. Karita, "Linear actuator," JP Patent 2002–027732, 2002.

[15] J. Wang, G. W. Jewell, and D. Howe, "Design optimisation and comparison of tubular permanent magnet machine topologies," *Proc. Inst. Elect. Eng.—Elect. Power Appl.*, vol. 148, no. 5, pp. 456–464, Sep. 2001.

[16] J. Wang and D. Howe, "Tubular modular permanent-magnet machines equipped with quasi-Halbach magnetized magnets—Part I:Magnetic field distribution, EMF, and thrust force," *IEEE Trans. Magn.*, vol. 41, no. 9, pp. 2470–2478, Sep. 2005.

[17] J. Wang and D. Howe, "Tubular modular permanent-magnet machines equipped with quasi-Halbach magnetized magnets—Part II: Armature reaction and design optimization," *IEEE Trans. Magn.*, vol. 41, no. 9, pp. 2479–2489, Sep. 2005.

[18] J. Wang, M. West, D. Howe, H. Z.-D. La Parra, and W. M. Arshad, "Design and experimental verification of a linear permanent magnet generator for a free-piston energy converter," *IEEE Trans. Energy Convers.*, vol. 22, no. 2, pp. 299–306, Jun. 2007.

[19] J. Wang, D. Howe, and Z. Lin, "Design optimization of short-stroke single-phase tubular permanent-magnet motor for refrigeration applications," *IEEE Trans. Ind. Electron.*, vol. 57, no. 1, pp. 327-334, 2010.

[20] N. Bianchi, S. Bolognani, D. D. Corte, and F. Tonel, "Tubular linear permanent magnet motors: An overall comparison," *IEEE Trans. Ind. Appl.*, vol. 39, no. 2, pp. 466–475, Mar. 2003.

[21] I-C. Vese, F. Marignetti, and M. M. Radulescu, "Multiphysics approach to numerical modeling of a permanent-magnet tubular linear motor," *IEEE Trans. Ind. Electron.*, vol. 57, no. 1, pp. 320-326, 2010.

[22] F. Cupertino and D. Naso, "An experimental comparison of adaptive and robust control methods for precise positioning with tubular linear motors," in *Proc. IEEE IECON*, pp. 71-76, 2010.

[23] F. Cupertino, P. Giangrande, G. Pellegrino, and L. Salvatore, "End effects in linear tubular motors and compensated position sensorless control based on pulsating voltage injection," *IEEE Trans. Ind. Electron.*, vol. 58, no. 2, pp. 494-502, 2011.

[24] S. Silaghiu and P. Mutschler, "Monitoring and control of a modular servo drive system based on PM linear synchronous motors," in *Proc. IEEE IECON*, pp. 900-905, 2010.

[25] R. Cao and K-S. Low, "Repetitive model predictive control of a precision linear motor drive," in *Proc. IEEE IECON*, pp. 1132-1173, 2007.

[26] R. Cao and K-S. Low, "A repetitive model predictive control approach for precision tracking of a linear motion system," *IEEE Trans. Ind. Electron.*, vol. 56, no. 6, pp. 1955-1962, 2009.

[27] Y-S. Huang and C-C. Sung, "Function-based controller for linear motor control systems," *IEEE Trans. Ind. Electron.*, vol. 57, no. 3, pp 1096-1105, 2010.

[28] C-C. Sung and Y-S. Huang, "Based on direct thrust control for linear synchronous motor systems," *IEEE Trans. Ind. Electron.*, vol. 56, no. 5, pp. 1629-1639, 2009.

[29] L. N. Tutelea, M. C. Kim, M. Topor, J. Lee, and I. Boldea, "Linear permanent magnet oscillatory machine: comprehensive modeling for transients with validation by experiments," *IEEE Trans. Ind. Electron.*, vol. 55, no. 2, pp. 492-500, 2008.

[30] J. G. Amoros and P. Andrada, "Sensitivity analysis of geometrical parameters on a double-sided linear switched reluctance motor," *IEEE Trans. Ind. Electron.*, vol. 57, no. 1, pp. 311-319, 2010.

[31] H. S. Lim, R. Krishnan, and N. S. Lobo, "Design and control of a linear propulsion system for an elevator using linear switched reluctance motor drives," *IEEE Trans. Ind. Electron.*, vol. 55, no. 2, pp. 534-542, 2008.

[32] L. Yu and T. N. Chang, "Zero vibration on-off position control of dual solenoid actuator," *IEEE Trans. Ind. Electron.*, vol. 57, no. 7, pp. 2519-2526, 2010.

[33] D. Li and H. Gutierrez, "Precise motion control of a hybrid magnetic suspension actuator with large travel," in *Proc. IEEE IECON*, pp. 2661-2666, 2008.

[34] R-J. Wai and J-D. Lee, "Comparison of voltage-source resonant driving schemes for a linear piezoelectric ceramic motor," *IEEE Trans. Ind. Electron.*, vol. 55, no. 2, pp. 871-879, 2008.

[35] A. Bellini, M. Colli, and E. Dragoni, "Mechatronic design of a shape memory alloy actuator for automotive tumble flaps: a case study," *IEEE Trans. Ind. Electron.*, vol. 56, no. 7, pp. 2644-2656, 2009.

[36] K. Yang, "Research and application of new inserted shape memory alloy actuators," *IEEE Trans. Ind. Electron.*, vol. 57, no. 8, pp. 2845-2850, 2010.

[37] Y. Fujimoto, T. Kominami, and H. Hamada, "Development and analysis of a high thrust force direct-drive linear actuator," *IEEE Trans. Ind. Electron.*, vol. 56, no. 5, pp.1383-1392, 2009.

[38] Y. Fujimoto, I. A. Smadi, H. Omori, and Y. Wakayama, "High thrust force direct-drive linear actuator and its application to musculoskeletal robots",

in *Proc. Int. Symp. on Application of Biomechanical Control Systems to Precision Engineering*, pp. 217-222, 2010.
[39] Y. Fujimoto, I. A. Smadi, H. Omori, K. Suzuki, and H. Hamada, "Modeling and control of a high-thrust direct-drive spiral motor," in *Proc. IEEJ IPEC*, 24F1-4, pp. 2222-2229, 2010
[40] Y. Fujimoto, Y. Wakayama, H. Omori, and I. A. Smadi, "On a high-backdrivable direct-drive actuator for musculoskeletal bipedal robots," in *Proc. IEEE AMC*, NF-003891, pp. 389-395, 2010.
[41] I. A. Smadi, H. Omori, and Y. Fujimoto, "On independent position/gap control of a spiral motor," in *Proc. IEEE AMC*, NF-001899, pp. 478-483, 2010.
[42] I. A. Smadi, H. Omori, and Y. Fujimoto, "On direct-drive motion of a spiral motor," in *Proc. IEEE IECON*, pp. 921-926, 2010.
[43] Y-M. Chen, S-Y. Fan, G-K. Chang, W-S. Lu, and R. L, Sheu, "Characterization of disk-type magnetically levitation motor," in *Proc. IEEE IECON*, pp. 1330-1335, 2007.
[44] S-M. Yang, C-L. Lin, "Levitation and torque control of a PM synchronous self-bearing motor with a single set of windings," in *Proc. IEEE IECON*, pp. 1033-1037, 2007.
[45] A. Chiba, D. Akamatsu, T. Fukao, and M. A. Rahman, "An improved rotor resistance identification method for magnetic field regulation in bearingless induction motor drives," *IEEE Trans. Ind. Electron.*, vol. 55, no. 2, pp. 852-860, 2008.
[46] S. Zhang and F. L. Luo, "Direct control of radial displacement for bearingless permanent-magnet-type synchronous motors," *IEEE Trans. Ind. Electron.*, vol. 56, no. 2, pp. 542-552, 2009.
[47] R-J. Wai and J-D. Lee, "Dynamic analyses and stabilizing control of linear magnetic-levitation rail system," in *Proc. IEEE IECON*, pp. 2213-2218, 2007.
[48] S-M. Yang, and M-S. Huang, "Design and implementation of a magnetically levitated single-axis controlled axial blood pump," *IEEE Trans. Ind. Electron.*, vol. 56, no. 6, pp. 2213-2219, 2009.
[49] S. M. Yang, "Electromagnetic actuator implementation and control for resonance vibration reduction in miniature magnetically levitated rotating machines," *IEEE Trans. Ind. Electron.,* vol. 58, no. 2, pp. 611-617, 2011.
[50] M. Rabiee and J. J. Cathey, "Verification of a field theory analysis applied to a helical motion induction motor," *IEEE Trans. Magn.*, vol. 24, no. 4, pp. 2125-2132, Jul. 1988.
[51] J. J. Cathey and M. Rabiee, "Verification of an equivalent circuit model for a helical motion induction motor," *IEEE Trans. Energy Convers.*, vol. 3, no. 3, pp. 660–666, Sep. 1988.
[52] T. Onuki, W. J. Jeon, and M. Tanabiki, "Induction motor with helical motion by phase control," *IEEE Trans. Magn.*, vol. 33, no. 5, pp. 4218-4220, Sep. 1997.
[53] J. H. H. Alwash, A. D. Mohssen, and A. S. Abdi, "Helical motion tubular induction motor," *IEEE Trans. Energy Convers.*, vol. 18, no. 3, pp. 362–369, Sep. 2003.
[54] L. Göbel and W. Hofmann, "Control of a rotation-thrust drive with helical motor," in *Proc. IEEE IECON*, pp. 1343–1348, 1997.
[55] S. M. Jang, S. H. Lee, H. W. Cho, and S. K. Cho, "Design and analysis of helical motion permanent magnet motor with cylindrical Halbach array," *IEEE Trans. Magn.*, vol. 39, no. 5, pp. 3007–3009, Sep. 2003.
[56] T. Iwasa and H. Satomi, "Linear/rotary combined motor," JP Patent 2006–311715, 2006.
[57] A. Hida, "Spiral motor," JP Patent 09–056143, 1997.

Issam A. Smadi (S'09-M'10) received the B.Sc. degree in electromechanical systems from Al-Balqa' Applied University, Jordan, in 2000, and the M.Sc. degree in control and power engineering from Jordan University of Science and Technology, Jordan, in 2003, and the Ph.D. degree in electrical and computer engineering from Yokohama National University, Yokohama, Japan, in 2009.

In 2003, he joined the Department of Electrical Engineering, Jordan University of Science and Technology, as a part-time instructor. Form 2009, he was a postdoctoral fellow in the Department of Electrical and Computer Engineering, Yokohama National University. Since 2011, he has been with the Fuji Electric Systems Co., Ltd, Tokyo, Japan.

His research interests include linear and nonlinear control theory, electric drive, robotics, and electric machines. Dr. Smadi is a member of the Institute of Electrical Engineers of Japan and of the Robotics Society of Japan.

Hiroko Omori received the B.E. and M.E. degrees in electrical and computer engineering from Yokohama National University, Yokohama, Japan, in 2009 and 2011, respectively.

Since 2011, she has been with the Toyo Electric Mfg. Co., Ltd., Yokohama, Japan. Her research interests include electric machines. Ms. Omori is a member of the Institute of Electrical Engineers of Japan and of the Robotics Society of Japan.

Yasutaka Fujimoto (S'93–M'98) received the B.E., M.E., and Ph.D. degrees in electrical and computer engineering from Yokohama National University, Yokohama, Japan, in 1993, 1995, and 1998, respectively.

In 1998, he joined the Department of Electrical Engineering, Keio University, Yokohama, Japan, as a Research Associate. Since 1999, he has been with the Department of Electrical and Computer Engineering, Yokohama National University, where he is currently an Associate Professor.

His research interests include actuators, robotics, manufacturing automation, and motion control. Dr. Fujimoto is a member of the IEEE-IES Technical Committee on Sensors and Actuators, the Institute of Electrical Engineers of Japan, and the Robotics Society of Japan.